



Integrated AHP and DInSAR Approach for Land Subsidence Hazard Assessment in Karaj Plain, Iran

Mojtaba Shiri, GholamReza Lashkaripour *, Naser Hafizi Moghaddas
Department of Geology, Faculty of Science, Ferdowsi University of Mashhad, Iran

Received: 03 April 2024, Revised: 08 July 2024, Accepted: 20 July 2024
© University of Tehran

Abstract

Land subsidence (LS) is a significant environmental issue affecting more than 50% of Iranian plains, particularly Karaj Plain located on the southern slopes of the Central Alborz, Iran. This study applied the Analytical Hierarchy Process (AHP) to create a LS hazard susceptibility map, considering factors such as groundwater drawdown, soil texture, alluvium thickness, distance between fault lines, and permeability. The resulting map was then compared with the Differential Interferometric Synthetic Aperture Radar method. The sensitivity mapping analysis revealed that 33.2% of the northwest-southeast direction in the studied area is classified as high- to very-high-risk. Moreover, analysis of Sentinel-1A images spanning eight years and three months (from October, 2014, to January, 2023) indicated that the maximum LS rate (158 mm/year) occurred in the central and northwestern parts of the study area, particularly within 200 to 300-meter thick layers containing significant clay layers. Over the past three decades, the Karaj plain has experienced groundwater depletion at an average annual decline of 0.9 meters. The five LS control points exhibited a strong negative correlation ranging from 66% to 88% with groundwater decline. Notably, this correlation suggests that maximum soil consolidation occurs with a two-year lag. Plus groundwater decline, a comparative study of two methods demonstrated that soil texture and alluvium thickness play a significantly influential role in asymmetric LS, especially considering the young age of the sediments and the presence of clay lenses. The accuracy of the generated LS hazard maps was validated using the ROC curve, achieving a high AUC of 0.773.

Keywords: AHP, DInSAR, Karaj Plain, Land Subsidence, Hazard Assessment

Introduction

Land subsidence (LS) refers to the sudden sinking or gradual settling of the ground surface, which happens due to the consolidation of sediment caused by an increase in effective stress. Several factors cause LS including the melting of ice, vibrations, the natural compaction of deposits, mining activities, and the extraction of groundwater. A staggering 6.3 million square kilometers of land worldwide is vulnerable to subsidence, Roughly 231,000 square kilometers of this vulnerable land are urban centers, housing nearly 2 billion people (Davydzenka et al., 2024). Studies have indicated that natural factors account for 23.08% of LS occurrences worldwide, while human-induced factors contribute to 76.92% (Bagheri-Gavkosh et al., 2021). LS is a significant geoenvironmental hazard that can cause a decrease in sediment void ratio, land settling, ground fissuring, and damage to infrastructure like buildings, pipelines, roads, railways, subways and permanent reduction in aquifers' storage capacity. Numerous researchers have extensively investigated various aspects of LS, and their valuable works have enhanced our understanding of this intricate phenomenon. In recent decades, the extreme employment of groundwater for urban and agricultural objectives is a major cause of LS in many areas around

* Corresponding author e-mail: Lashkaripour@um.ac.ir

the world (e.g. Salehi Moteahd et al., 2019; Jahangir et al., 2020; Ty et al., 2021; Ghahfarokhi et al., 2023; Chen et al., 2023; hatterjee et al., 2023; Hussain et al., 2024). Ozdemir (2016a, b) investigated the distribution of LS in Turkey and showed that the rate of subsidence is directly related to the sediment thickness, distance to the river and the fault. The InSAR technique is well-suited for monitoring how aquifer systems respond both elastically and inelastically to fluctuations in groundwater levels. Moreover, it offers fresh perspectives on the influence of lithological characteristics and geological structures in aquifers (e.g. Hoffmann et al., 2001; Li and Li., 2023; Motagh et al., 2008; Zuccarini et al., 2023). Studies executed by Ciampalini et al. (2014) and Zhou et al. (2020) demonstrated the capability of these methods to achieve accuracy within the mm to cm range in unsurpassed spatial sampling density. InSAR analysis reveals significant spatial variability in LS rates across the southwestern region of Bangladesh. These rates range from 3 to 20 millimeters per year, with higher rates observed in specific locations. This spatial variation highlights the influence of various factors on subsidence, including the weight of overlying sediments, natural consolidation processes, compaction of existing sediments, regional tectonic movements, and human activities (Shahoriar Sarker et al., 2024).

There are several methods available for the analysis, prediction, and monitoring of LS. Accurately quantifying LS presents a significant challenge due to the multifaceted nature of the phenomenon and the complex interplay of various influencing factors. To address this challenge, researchers have increasingly embraced the application of machine learning techniques. These methods leverage existing local subsidence measurements alongside geospatial data to identify areas susceptible to subsidence. This data-driven approach has been demonstrably successful in various locations around the globe, including Iran (Mohammady et al., 2019), the United Arab Emirates (Elmahdy et al., 2022), Greece (Iliia et al., 2018), Indonesia (Hakim et al., 2020) and the United States (Smith & Majumdar, 2020). Notably, these studies incorporated relevant predictor maps encompassing climate, topography, geological characteristics, soil properties, and hydrological conditions specific to the investigated area. Faryabi et al. (2023) introduced a fuzzy logic-based method to map the susceptibility of LS in the Jiroft plain located in the southern part of Iran. The proposed model incorporated various hydrogeological factors including groundwater pumping rate, geology, saturated and unsaturated media, groundwater drawdown, soil and aquifer type, transmissivity, aquifer thickness, and distance to faults. Their findings revealed that areas exhibiting the greatest susceptibility to LS are characterized by low-permeability soils, thick aquifers, high rates of groundwater pumping, and close proximity to faults. Numerous models were developed to assess the risk of LS, such as (DSC-ADTree), Artificial Neural Network (ANN), DL models (e.g., CNN and LSTM), and receiver operating characteristic (ROC), (Zhao et al., 2024; Riseh et al., 2023; Rahmani et al., 2024; Zhang et al., 2023).

In Iran, LS poses a significant challenge in the central and northeastern parts of the country due to excessive groundwater extraction. Evaluating the rate and factors influencing this phenomenon is crucial. Within a 10-kilometer radius to the west and south of the Karaj Plain, has experienced extensive ground cracks caused by LS, resulting in severe damage to infrastructure and agricultural land (Mahmoudpour et al., 2016; Mehrnoor et al., 2023). Several researchers have therefore investigated this phenomenon in the Karaj Plain. safari et al. (2016) used the Interferometric Synthetic Aperture Radar (InSAR) technique to assess the rate of LS in the Karaj-Shahriar Plain. The study period was from 2003 to 2010. Time series analysis with short baselines was employed in DORIS software to obtain the average annual subsidence rate, which reached a maximum of 136 mm/year. Results showed that the amount of ground surface elevation change in the Karaj metropolis ranged from -145 to 15+ millimeters. The most significant subsidence occurred in Mehrshahr, with subsidence ranging from 100 to 145 millimeters. This subsidence was primarily attributed to increased groundwater withdrawal and decreased precipitation (Ranjbar & Fathollahzadeh, 2022).

Previous studies in the Karaj Plain have not utilized the AHP methodology to create LS hazard maps. Given the lack of a comprehensive study in the Karaj Plain that considers crucial parameters beyond groundwater depletion in relation to land subsidence, it is imperative to conduct research in this area. It is crucial to comprehend the factors contributing to LS and to devise effective strategies for its mitigation. This study evaluated the impacts of fault distance, groundwater level decrease, permeability, alluvium thickness, and soil grain size on ground subsidence in the Karaj Plain. A flowchart outlining the overall research process is presented in Figure 1. In the first step, the effects of these parameters on subsidence were evaluated by AHP. In the second step, the actual subsidence of the plain was estimated by the differential interferometric synthetic aperture radar (DInSAR) approach. In the third step, the results of AHP were validated by comparing them with the results of DInSAR.

Study area

The Karaj Plain is situated 20 km west of Tehran, in the Alborz Province, in the north of Iran. It is bounded by mountains on two sides, the north and the south (Figure 2a and b). The plain covers an area of approximately 468 km² and is home to several cities, including Karaj, Kamal Shahr, Mohammad Shahr, Mehr Shahr, and Mahdasht, with a total population of over one million people in 2021 (The Statistical Center of Iran, 2021). Besides residential zones in both urban and rural areas, the plain is also home to several industrial areas, plants, roads, railways, and thousands of groundwater withdrawal wells. The main river in the plain is the Karaj River, which flows through the center of the plain. The plain is subjected to the ground subsidence which caused several significant disasters including damage to buildings and linear structures (roads), as well as ground surface cracking in the center of the plain (Figure 2c and d). The tension cracks are oriented north-south and are several meters long and deeper than 0.1 meters.

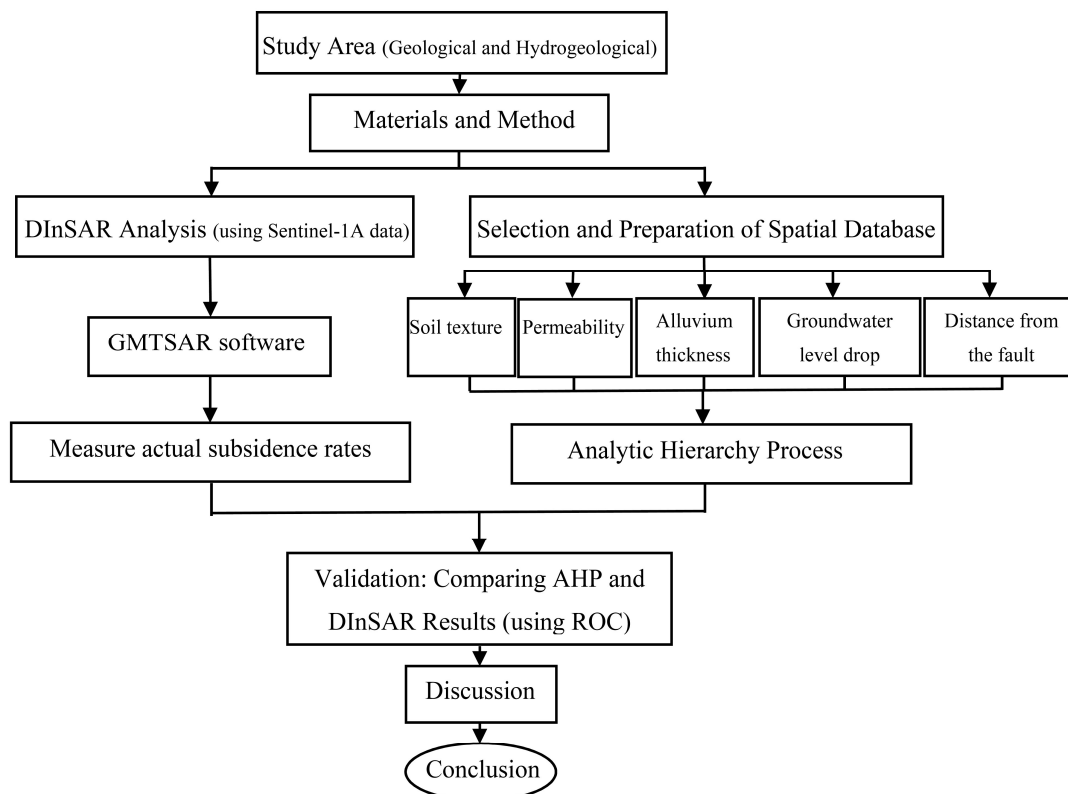


Figure 1. Flowchart of the Study Process

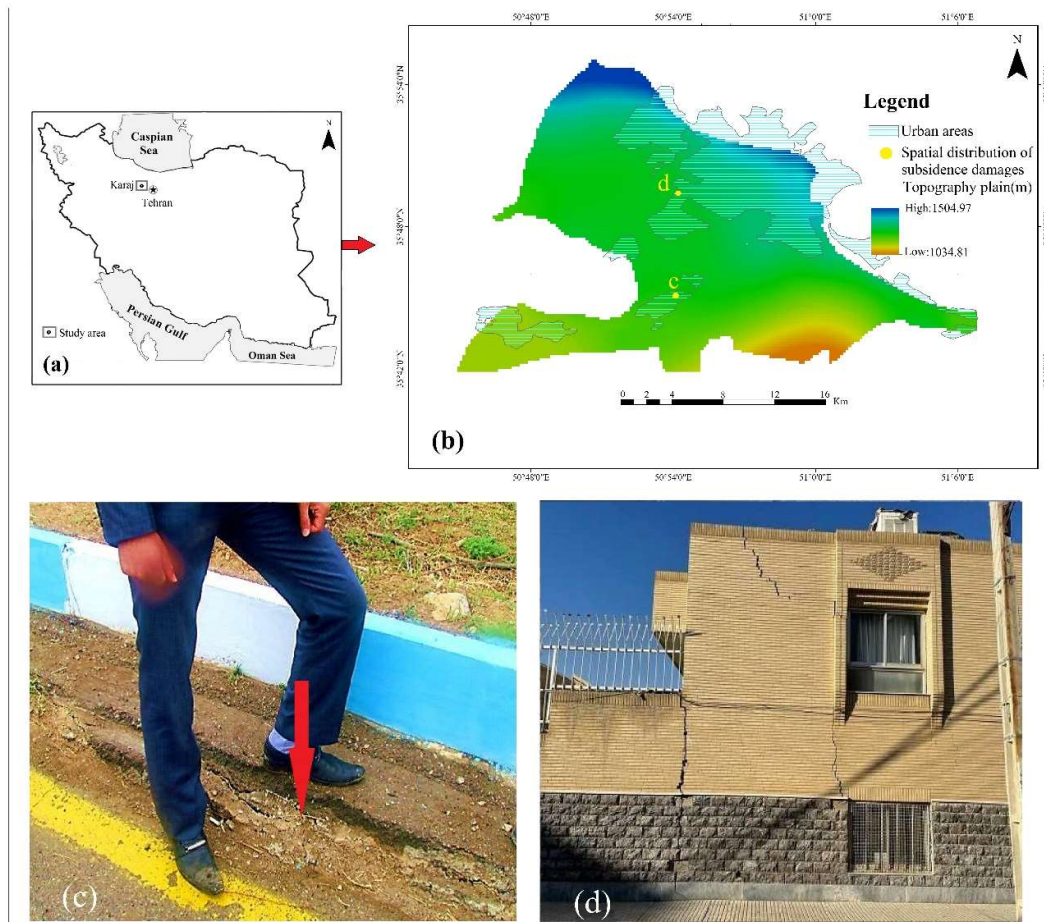


Figure 2. a: Sampling points in Iran map, b: Karaj Plain and the InSAR satellite image analysis area, c: Crack development due to the subsidence, and d: Damage to the buildings

Geological and hydrogeological conditions in Karaj Plain

Geology of the area

The tectonic features of this region generally follow the conditions of the central Alborz. From a geological perspective, the Karaj tectonics are primarily composed of sedimentary rocks and detrimental (or clastic) sediments (Abdolali, 1991). The Karaj Plain deposits are situated in the foothills of the southern part of the Alborz Mountain Range, which is characterized by tectonic activity due to the convergence of the Arabian and Eurasian plates. The northern heights of the study area are composed of green tuff massif, while the southern heights are composed of andesite and Miocene rocks. The Karaj Formation was formed in the Eocene as a result of the Pyrenees phase. It has a thickness of more than 3,300 meters. The Red Formation is considered to be the bedrock in the south and west of the Karaj site (Figure 3).

The most recent major tectonic movements in the Alborz region took place during the late Pliocene to early Pleistocene period, resulting in faulting and moderate thrusting in the mountains. This geological activity led to the formation of the Hezardareh Formation (also known as Formation A) (Rieben 1995). This division Rieben, Was the basis for further studies and since then have not been major changes in this classification. The Karaj and Kordan rivers, along with other rivers and seasonal floods, have caused erosion in the Alborz Mountains. This erosion has resulted in the deposition of Quaternary alluvial sediments on the southern slopes of the mountains. The city of Karaj is situated on these relatively soft and young deposits.

Rieben (1955) conducted a study on the stratigraphy, lithology, and age of these Quaternary alluvial deposits, dividing them into four formations:

- Hezardareh Formation (A= Q1)
- Kahrizak Formation (B= Q2)
- Alluvial sediments of Tehran Formation (C= Q3)
- Recent Sediments Formation (D= Qal)

The Hezardareh Formation, a deposit of old alluvial material located on the margins of the highlands, consists primarily of rubble, gravel, and weak silty-clay cement. This formation is characterized by low porosity and permeability, hindering the lateral flow of groundwater within the aquifer. The Hezardareh Formation is distributed throughout the northwestern region of Karaj Plain. The Kahrizak Formation comprises younger alluvial deposits and elevated riverside terraces. Granulometry reveals a composition of sand, gravel, and slate fragments. Notably, this formation exhibits higher permeability compared to the Hezardareh Formation. The Kahrizak Formation underlies the majority of the plain, encompassing the central, eastern, southern, and southwestern regions. The Tehran Alluvial Formation is formed through the erosion of older formations and consists of alluvial fan and floodplain deposits. This formation covers a significant portion of the low-lying areas of the plain. Its considerable thickness and high permeability make it the main aquifer of the plain. The Recent Sediments Formation represents the youngest Quaternary deposit found in the Karaj Plain.

Hydrogeology of the area

The aquifer within the Karaj Plain spans approximately 376.9 km² in area. Karaj County experiences an average annual precipitation of 247.3 millimeters and an average annual temperature of 14.4 degrees Celsius. Emerging from the mountains, the Karaj River has given rise to the Karaj alluvial fan. Over time, sedimentation and compaction of sediments on the surface of the alluvial fan by the Karaj River have caused its surface to rise and facilitated the movement of channels towards the southeast. These repeated channel shifts have ultimately led to the formation of the large and present-day Karaj alluvial fan. The primary aquifer in the plain is the Tehran Alluvial Formation, which is characterized by its extensive coverage, considerable thickness, and high permeability. It consists of Quaternary alluvium, with coarser sediments near the highlands and finer sediments in the central plain. The thickest layer of alluvium, around 300 meters, is situated in the central part of the plain, running in a northwest-southeast direction. In the western and southwestern regions of the plain, the aquifer exhibits a layered structure, with coarse-grained layers separated by aquitard layers, forming confined aquifers. In the rest of the plain, the aquifer is unconfined. The bedrock underlying the Karaj Plain follows a northwest-southeast orientation, gently sloping towards the southeast, resulting in a distinctive horseshoe shape for the plain. The depth of the bedrock varies across the plain, with shallower depths in the two branches of the horseshoe and deeper depths in the central section. The medium storativity coefficient in the study area is estimated to be around 5%. The maximum coefficient of transmissivity ranges from 3,000 to 5,000 m²/day in the center-south region of the plain, while the minimum is 400 m²/day in the southwest. For more than 30 years, from 1992 to 2022, excessive extraction of groundwater from the Karaj Plain has led to a significant decline in water levels, reaching a total drop of 27.15 meters. On average, this corresponds to a yearly decrease of 0.9 meters. As shown in Figure 3, water inflow fronts pass through the northern, western, and northeastern boundaries, while water outflow fronts pass through the eastern and southwestern boundaries. This information is based on data provided by the Geological Survey of Iran (2020), the Alborz Regional Water Company (2022), and the Alborz Water and Wastewater Company (2019). This makes the central plain more susceptible to subsidence.

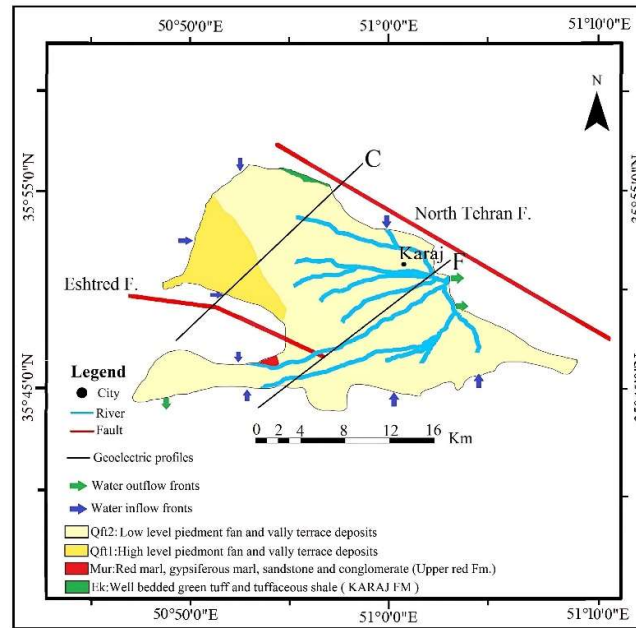


Figure 3. Geological map of the study area and locations of geoelectric profiles C and F (Khezri et al., 2022; Geological Survey and Mineral Exploration of Iran, 2020)

Materials and methods

Materials

The hazard susceptibility maps for LS were created by utilizing remote sensing images and additional data, such as groundwater level drop, soil texture, alluvium thickness, distance from the fault, and permeability, collected from a variety of sources. In this research, the European Space Agency's state-of-the-art high-resolution satellite Sentinel-1A was used to collect the data. This C-band SAR satellite utilizes a new terrain observation with progressive scan SAR (TOPSAR) imaging mode to achieve a 12-day return period and has a wide observation range of 250 km × 250 km at medium resolution. Fortunately, the obtained observations from Sentinel-1A are complimentary.

Additionally, SAR images were captured in a descending orbit using an Interferometric Wide swath (IW) TOPS mode with VV polarization. Then, the GMTSAR software was executed for the processing.

Methodology

The LS hazard sensitivity maps were developed by AHP technique. The Analytic Hierarchy Process (AHP) was employed to develop LS hazard sensitivity maps. AHP is a multi-criteria decision-making technique that facilitates the prioritization of factors influencing LS susceptibility. In this study, the AHP hierarchy was structured with the main criterion being LS hazard, followed by sub-criteria representing various some physical parameters. Various Geo-environmental parameters contribute the production of LS hazard sensitivity mapping using GIS tools. Several studies have looked at geomorphic features in LS hazard studies, with parameters such as groundwater drawdown, soil texture, alluvium thickness, distance between fault lines, and permeability (e.g. Mohammady et al., 2019; Abdollahi., 2019; Rezaeia, M et al., 2020; Smith & Majumdar, 2020; Hakim et al., 2020; Elmahdy et al., 2022).

The selection of factors for the AHP model in the Karaj region was based on a comprehensive

understanding of LS processes, the availability of relevant data, and the specific geological and environmental characteristics of the study area. After identifying the key factors influencing LS, the AHP method utilizes a two-step process to determine their relative importance. First, factors are compared pairwise based on their influence on LS susceptibility, using a scale reflecting one factor's dominance over another. These comparisons are then compiled into a comparison matrix, which captures the overall relative importance of each factor compared to all others. Finally, mathematical calculations are applied to this matrix to derive weights for each factor, effectively translating expert judgment and pairwise comparisons into quantitative values that reflect the relative contribution of each factor to LS susceptibility. Also, ground deformations were produced by the DInSAR method.

Analytic Hierarchy Process (AHP)

Saaty (1977) introduced an analytical method called AHP. This semi-quantitative method is employed to address intricate problems by dividing them into a hierarchical structure of factors and subsequently comparing these factors pairwise. The AHP assigns a scale ranging from 1 to 9 to express the relative importance of each factor (Saaty, 1980a, b). Table 1 demonstrates a standard scale for conducting pairwise comparisons.

In the matrix, the elements a_{ij} represent the values obtained from the paired comparisons between factor i and factor j . Meanwhile, the diagonal elements represent the fact that each factor is considered equally important to itself, resulting in a value of one. The matrix contains the evaluation results provided by the expert decision-makers, as indicated by Eq. 1.

$$A = \begin{bmatrix} 1 & 1/a_{12} & \dots & 1/a_{1n} \\ a_{21} & 1 & \dots & 1/a_{2n} \\ \vdots & \vdots & \dots & \vdots \\ a_{n1} & a_{n2} & \dots & 1 \end{bmatrix} = \begin{bmatrix} 1 & a_{12} & \dots & a_{1n} \\ a_{21} & 1 & \dots & a_{2n} \\ \vdots & \vdots & \dots & \vdots \\ 1/a_{1n} & 1/a_{2n} & \dots & 1 \end{bmatrix} \tag{1}$$

Once the comparison matrix was constructed, the consistency of the matrix was assessed using the eigenvalue method, and the consistency ratio (CR) was calculated accordingly, as depicted in Eq. 2. Saaty (1980a, b) has indicated that for a randomly generated comparison, the CR tends to approach 1, and as the CR approaches 0, greater consistency is achieved. In general, a CR value of ≤ 0.1 is considered acceptable.

Table. 1 Pair-wise comparisons based on a standard scale (Saaty, 1980a, b)

Importance	Definition	Description
1	Equal important	Two parameters hold equal significance
3	Moderate important	One parameter is slightly favored over the other.
5	Strong important	One parameter is Strongly favored over the other
7	Very strong important	One parameter is very strongly favored over the other
9	Extreme important	Evidence favoring one element over another is the highest possible order of affirmation
(2,4,6,8)	Intermediate values	

$$C.R = \frac{C.I}{R.I} \quad (2)$$

As seen in (Eq. 3), CI represents the consistency index, which is computed using a specific formula. On the other hand, random index (RI) refers to the random index derived from the comparison matrix.

$$C.I = \frac{\lambda_{max} - n}{R.I} \quad (3)$$

In the given equation, n represents the order or size of the matrix, RI is a measure of the consistency of the pairwise matrix produced randomly, and λ_{max} denotes the principal value of the matrix. The value of RI depends on the size of the matrix and can be categorized into 10 classes from RI=0 to 1.49

AHP analysis based on selected physical parameters

This study utilized previous research to select and prepare a spatial database consisting of five physical parameters: Groundwater level drop, soil texture, alluvium thickness, distance from the fault and permeability (Figure 6). Moreover, weights derived using the AHP method were employed to rate the relative importance of both classified raster layers and parametric maps (Tables 2 and 3). A concise overview of all parameter which affect LS have presented in the following sections.

Table 2. AHP pairwise comparison matrix

Parameters	Classes	Pair wise comparison matrices						Eigen values	CR
Distance from Fault line (m)	0-250	1						0.5128	0.05
	250-500	0.33	1					0.2615	
	500-750	0.5	0.33	1				0.1290	
	750-1000	0.14	0.5	0.33	1			0.0634	
	>1000	0.11	0.14	0.5	0.33	1		0.0333	
Groundwater Level Decline during the years 2014-2022 (m)	32-25	1						0.2916	0.00
	25 – 19	0.33	1					0.2081	
	19-13	0.33	1	1				0.2081	
	13-7	0.5	0.33	0.33	1			0.1252	
	7-2	0.5	0.33	0.33	1	1		0.1252	
Alluvium Thickness(m)	<2	0.14	0.5	0.5	0.33	0.33	1	0.0417	0.03
	>300	1						0.4691	
	250-300	0.33	1					0.2010	
	200-250	0.33	1	1				0.2010	
	100-200	0.5	0.33	0.33	1			0.0862	
Permeability	50-100	0.14	0.5	0.5	0.33	1		0.0427	0.00
	Qft1	1						0.5239	
	Qft2	0.33	1					0.2707	
	Upper red Fm (Mur)	0.5	0.5	1				0.1354	
Soil texture	KARAJ FM (Ek)	0.14	0.14	0.14	1			0.0700	0.04
	Silt- lean Clay	1						0.5650	
	Clayey Sand	0.33	1					0.2622	
	Poorly Graded Sand	0.5	0.33	1				0.1175	
	Poorly Graded Gravel	0.14	0.5	0.33	1			0.0553	

Table 3. Parameters matrix, wise weights and consistency ratio using AHP

Parameters	Pair wise Comparison Matrices					Weights	CR
Groundwater Level Decline (m)	1					0.3621	
Soil texture	1	1				0.3621	
Alluvium Thickness(m)	0.33	0.33	1			0.1607	0.03
Distance from Fault Line (m)	0.5	0.5	0.33	1		0.0762	
Permeability	0.14	0.14	0.5	0.33	1	0.0389	

Groundwater Level Drop

The occurrence of groundwater drawdown will lead to an elevation in effective pressure, a decrease in porosity, and an acceleration in subsidence rate, particularly in regions that contain clay layers. In this study, thirty piezometric wells were selected to evaluate the effectiveness of groundwater level as a parameter in subsidence rate. The variations in groundwater levels belong to the period of 2014–2022. Deep water wells, geophysical studies, and upstream and downstream piezometers suggest that the water Table. in the second aquifer, which plays a major role in land subsidence, is located at a deeper depth. However, the piezometers in the center of the plain were likely drilled into a shallow suspended aquifer.

Soil texture

Soil texture plays a significant role in LS. Clay soils are particularly vulnerable to subsidence due to their higher water content and greater susceptibility to compaction when water is drained. To obtain a more detailed understanding of the subsurface, three cross-sectional profiles were examined in a northwest-southeast direction in the study area (Figure 9). Figure 4 shows section A-A', which is composed of initial alluvial fan deposits that lie along the North Karaj Fault and Karaj City located at the center of this section. Examination of borehole logs shows that western and eastern sections are mainly composed of coarse-grained deposits. In the center of the section, which slopes slightly to the northwest, fine-grained deposits are observed. The bedrock of the western and southeastern sections of the section is composed of Miocene marl or clay, and the center probably consists of conglomerates of the Hajar Valley or terraces A (late Miocene-Pliocene).

Figure 4 shows section B-B', taken from the center of the alluvial fan deposits, which have a considerable thickness. Approximately 30% of soil in this section composes of fine-grained deposits, while the remaining part composes of coarse-grained materials. Moving from the northwest to the southeast, coarse-grained deposits with a small percentage of fine-grained deposits are first observed. Then, about 60% of fine-grained silt and clay deposits with intermittent sand are observed. Finally, from the central section onwards, the deposits again become coarse-grained with about 10% fine-grained deposits. None of the seven boreholes in this section, even those deeper than 250 meters, have reached bedrock. The bedrock of the western and southeastern sections of this section probably consists of Miocene marl or clay, and the center probably consists of conglomerates of the Hajar Valley or terraces A (late Miocene-Pliocene).

Figure 4 shows section C-C', which shows alluvial deposits with a thickness of over 300 meters in a northwest-southeast direction (along the axis of the Buin anticline). In the southeastern half of the section, coarse-grained deposits with a small percentage of fine-grained deposits are the dominant constituent. In the central part of this section, fine-grained and coarse-grained deposits are alternatively seen, eventually ended to fine-grained soils. The bedrock of the northwestern section of C-C' section is likely composed of Miocene marl or clay, and the center part of this section to the southeast probably consists of conglomerates of the Hajar Valley or terraces A (late Miocene-Pliocene).

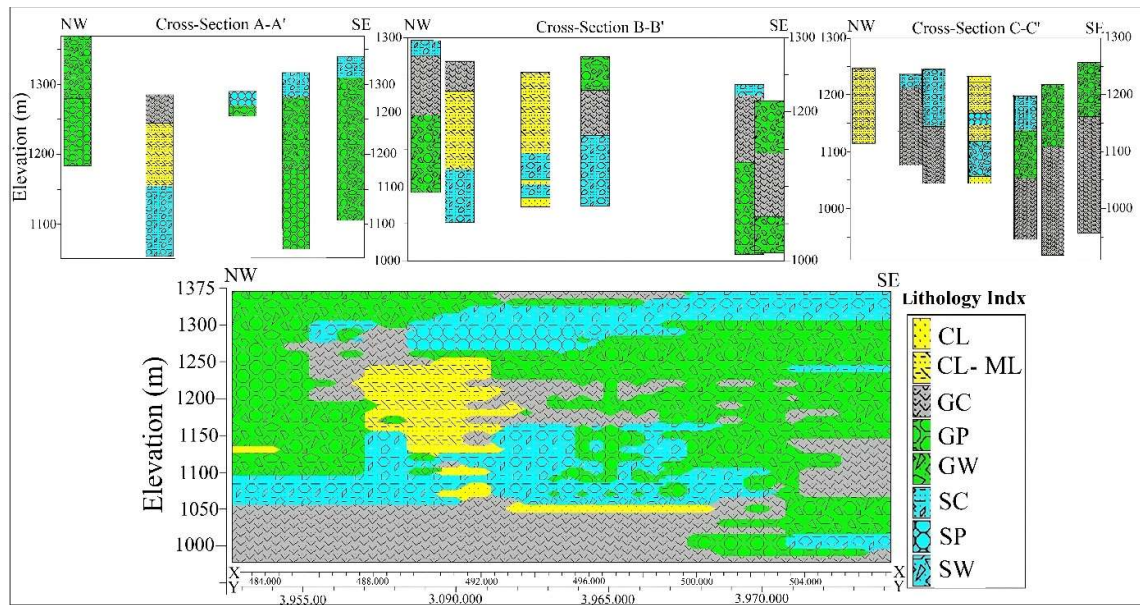


Figure 4. cross sections (A–A', B–B' and C–C') and Two-dimensional profiles of sections

The results of the studies, demonstrated in the form of a two-dimensional profile in Figure 3, showed that there is a direct relationship between fine-grained deposits and LS in this plain.

Based on 19 well logs and geoelectric data, the soil texture of the Karaj Plain has been divided into four categories. Sediments with a coarse grain size have accumulated in the vicinity of the hills, whereas sediments with a finer grain size have settled further away from the hills.

Alluvium Thickness

There is a positive correlation between the thickness of the compressible layer and the magnitude of LS. This implies that the increasing in the thickness of compressible layer will develop the LS rate (Li et al. 2017). The Karaj geoelectric profiles are in the northeast-southwest direction (Figure 3). From these profiles, profiles C and F were selected for the study of the Karaj plain (Figure 5). Profile C, borehole number 29M.45D, was drilled to a depth of 120 meters near electrical sounding number 152. Soils in this borehole is composed of clay, sand, and gravel up to a depth of 47 meters, and then sand, gravel, and clay up to a depth of 120 meters. According to geophysical results, the bedrock of the region has a resistivity of 30 ohm-meters and is located at a depth of 300 meters.

Profile F, along the axis of the existing anticline, has sedimentary layers with a maximum thickness of about 300 meters overlying a horizon of A terrace deposits. From the center to the southwest, alluvial deposits become finer-grained, and the thickness of the deposits in the southwest reaches about 50 meters, decreasing to a minimum value on igneous rocks. Borehole number 32R.1D, located in the southwestern part of the plain, was drilled to a total depth of 91.5 meters. The electrical resistivity of the ground in this region ranges from 20 to 30 ohm-meters up to a depth of 62 meters, and then changes to 100 ohm-meters from 62 to 90 meters. After this depth, it decreases to a resistivity of 10 ohm-meters to the bedrock of the region.

Alluvium thickness map, which is prepared using the geoelectric soundings, the deep water wells (There are 19 deep water wells with a normal distribution in the plain. The depths of these wells range from 132 to 300 meters, with an average depth of 220 meters) and information of the piezometers (C.G.G Company, 1964-1965; Alborz Regional Water Company, 2022). The thickest alluvium in the plain, located in the center of the plain (south of Karaj city), has a thickness of more than 300 meters, while the thinnest alluvium layer has a thickness of at least

50 meters in the southwest. Significantly thick layers of fine-grained sediment that are prone to subsidence are located in the center and west of the plain.

Distance from the fault

The extent of LS induced by a fault is influenced by various factors, including the size, type, and rate of movement of the fault, as well as the characteristics of the soil in the region. When faults are large and exhibit rapid movement, they can result in significant LS. Fault structures create fractures and gaps within the geological layers, which enhance the potential for drainage and groundwater infiltration. This, in turn, increases the likelihood of subsidence. In the study area, the North Tehran Reverse Fault is situated in the northern part, while the Eshtehard Reverse Fault is located in the southern part (Rieben, 1995).

In a recent study, Shastri et al. (2023) found that LS in Kolkata, India is a serious problem caused by groundwater depletion and increased seismic hazard, according to two decades of InSAR and GPS measurements.

Permeability

The amount of LS that occurs depends on the type of soil and rock that is being compacted. Soils and rocks with high permeability, such as sand and gravel, are more likely to compact than those with low permeability, such as clay. This is because materials with high permeability can easily absorb water. When the water Table. drops, these materials lose the support of the water. As a result, they compact and sink. In conclusion, soil permeability is a key factor in LS (USGS, 2023).

The permeability of water in the high-level piedmont fan and valley terrace deposits is highest in the Quaternary deposits (Qft1), followed by relatively high permeability in the low-level piedmont fan and valley terrace deposits (Qft2). However, formations such as red marl, sandstone, gypsiferous marl, conglomerate of Miocene age (Upper red Fm (Mur)), and well-bedded tuffaceous shale and green tuff of Eocene age (KARAJ FM (p)) exhibit low permeability. Generally, the formations in the study area can be categorized into two main types: soft and hard or cemented formations. Among these, geological factors have the most significant impact on land permeability, as they undergo minimal changes compared to climate, topography, and vegetation factors in the plain. The permeability of the formations is influenced by various factors, including climate, topography, vegetation, and geological characteristics, with special emphasis on effective porosity (Ghabadi, 2013). Generally, an increase in permeability decreases the LS rate.

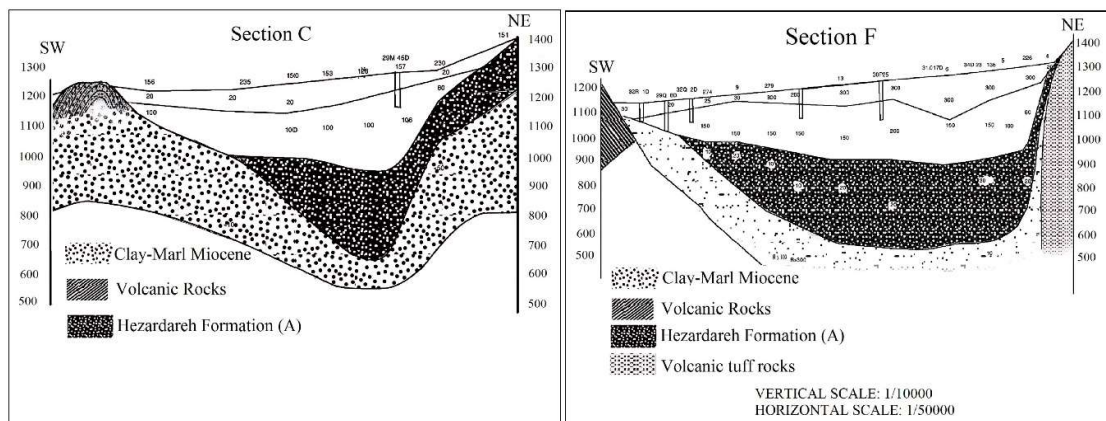


Figure 5. Geoelectric profiles C and F

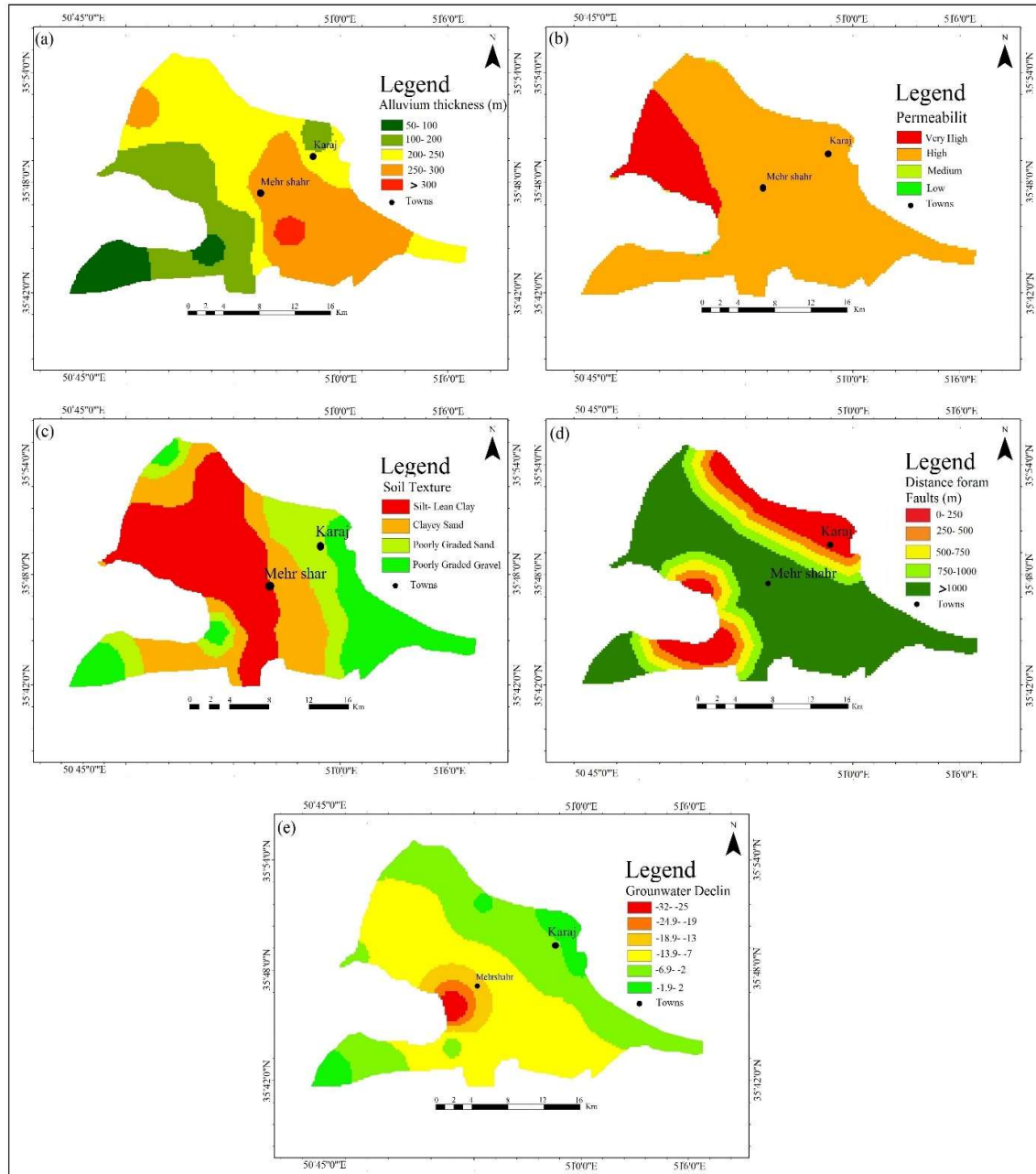


Figure 6. Thematic Map of LS Hazard Sensitivity Parameters: a) Alluvium Thickness, b) permeability, c) Soil texture, d) Distance from Fault, e) Groundwater Level Decline

By adding up the weight of each parameter multiplied by the class weight assigned to that parameter, the LS Hazard Sensitivity Index (LHSI) value was calculated for every pixel, as shown in Eq. 4.

$$HSI = \sum_{i=1}^n (WiRi) \quad (4)$$

In the given equation, HSI represents the LS hazard sensitivity index for the specific pixel being analyzed. W_i denotes the weight assigned to parameter i , while R_i represents the criteria score associated with parameter i

DInSAR data and processing

Sentinel-1A SAR images were utilized to generate a ground deformation map of the study area by the DInSAR method. DInSAR is a powerful tool for monitoring LS. There are several different data processing methods that can be used for DInSAR, each with its advantages and disadvantages. The choice of data processing method depends on the specific application and the available data (Pepe & Calò, 2017). A study by Zheng et al. (2023) used InSAR data and the Peck model to examine surface subsidence disasters in Xuzhou City, China, from 2014 to 2018. They found that the areas with the most severe subsidence were those with high groundwater pumping rates and areas with soft soils.

The descending tracks of Sentinel-1A images from the TOPS data sets covering a period of 9 years from 2014 to 2023 were analyzed using SLC (Single Look Complex) products. Using one-month interval master and slave image co-registration, 183 interferograms were developed. A sample interferogram superimposed on the DEM is presented in Figure 7.

After terrain correction of the final vertical displacement map, the mean value of the displacement map was measured for the study area, because the determined vertical displacement values are relative.

Results and discussion

LS hazard sensitivity index map

Based on the results, the maximum consistency ratio (CR) is 0.05, indicating good consistency within the judgment matrix (below 0.1). The groundwater level in the west of the Karaj Plain has dropped by a maximum of 71 meters, while the easternmost part of the Plain has seen an increase of 5 meters. The average decrease in groundwater level in the Karaj Plain is about 0.9 meters annually, according to studies by the Regional Water Company of Alborz.

In various geological and hydrogeological conditions, the presence of multi-layered aquifer systems, including thick compressible clay layers and deep confined aquifers, can contribute to the development of LS (Wang et al., 2019).

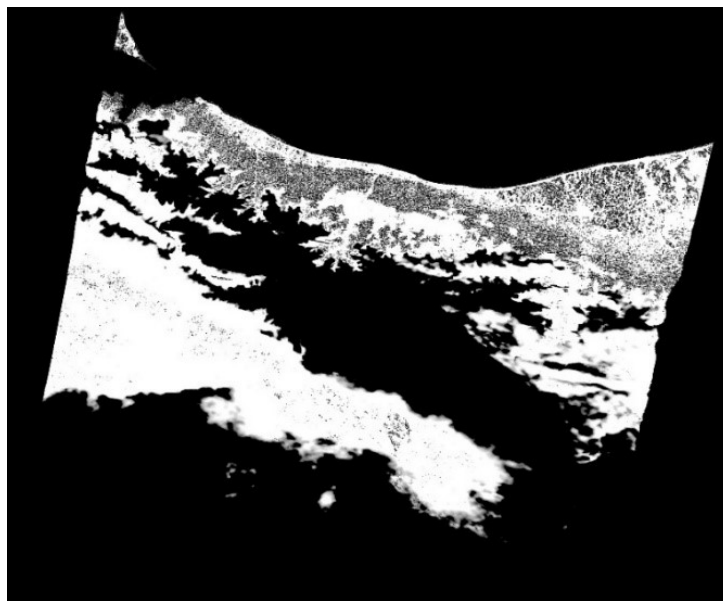


Figure 7. Interferometric phase for an ascending track data over the July 20, 2020– August 13, 2020

It is worth noting that the piezometers located in the west and southwest of the plain have a low groundwater depth and do not show significant fluctuations. For example, the piezometer in Husseinabad Mehrshahr (level 1256 meters) is located at a lower level than the piezometer in Tarbiat Moallem (level 1285 meters). However, the water level in September 2003 in the Husseinabad piezometer was 1241 meters, and in the Tarbiat Moallem piezometer 1208 meters. If these two piezometers are located in a single aquifer, such conditions are not hydraulically correct. This is because the southern highlands do not play a role in the aquifer recharge, and the Husseinabad Mehrshahr piezometer is probably located in the first layer. Since the depth of the Husseinabad Mehrshahr piezometer is less than the surrounding piezometers, there is a possibility that the aquifer has two layers. Taking into account that the piezometric pressure in the second layer has decreased and the second layer is in a free state, it is expected that subsidence in Mehrshahr will be more than in other parts of the plain. In the study area, the soil texture is divided into four groups from the heights to the center of the plain, respectively:

- Poorly-graded gravel and well-graded gravel (GP, GW)
- Poorly-graded sand and well-graded sand (SP, SW)
- Silty clayey gravel and silty clayey sand (GC, SC)
- Silty clayey (CL-CL, ML)

In areas with no fine-grained soils, such as the southeastern plain (north of Fardis), there is no significant subsidence despite the high depth of groundwater and high soil thickness. Accordingly, the maximum and the minimum alluvial thickness were 340 meters in east Mohammadshahr and 50 meters in Mahdasht, respectively. Distance from the faults has the highest susceptibility for distances less than 1 km and the lowest susceptibility for distances greater than 10 km. The permeability of the Qft1 formation is excellent, the permeability of the Qft2 formation is good, and the permeability of the other alluvial formations of the Karaj Plain is medium to low.

The LS hazard sensitivity index map was created by combining the weighted sum of the five mentioned parameters (Figure 8).

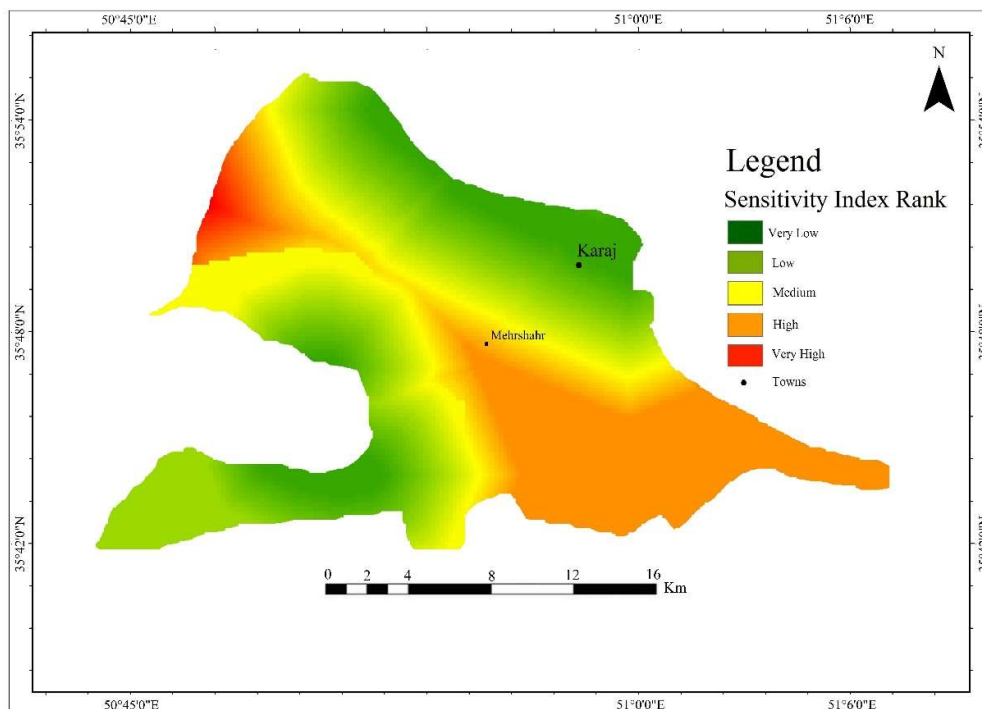


Figure 8. LS hazard Sensitivity map generated by the Fuzzy- AHP approach

The fuzzy approach in ArcGIS was utilized to categorize the obtained LS hazard sensitivity map. The results of the sensitivity mapping indicated that 17.48% of the study area was at very low risk, 24.99% at low risk, 23.7% at medium risk, 31.7% at high risk, and 2.13% at very high risk. In general, areas with a high to very high risk of LS are located in the NW-SE direction, and the northeastern part of the plain has the highest probability of LS.

DInSAR processing result

To eliminate the influence of topography, the SRTM (Shuttle Radar Topography Mission) Digital Elevation Model (DEM) was utilized. This process involved removing the topographic effect from the interferogram phase. The local coherence in the image has an impact on the attribute of the interferogram phase. In DInSAR processing, the coherence was calculated by the interferometric SAR pairs to determine the phase noise. A coherence map was generated for the entire scene by applying a shifting window over the SAR image. It is worth mentioning that the coherence range is between 0 and 1, where a value of 0 indicates that the interferometric phase is mostly comprised of noise, while a value of 1 shows that the interferometric phase is free of noise.

The wrapped phase information in DInSAR interferogram fringes changes from $-\pi$ to π . As seen in the displacement map, the negative values show areas experiencing subsidence, and positive values reveal areas experiencing uplift. Figure 9 shows the vertical annual displacement map with a maximum subsidence of 158 mm/year. Based on the vertical displacement maps, it can be concluded that the DInSAR approach is effective and suitable for analysis, especially in regions where the interferogram fringes are clear and distinguishable.

Cross-validation of the two methods using the ROC curve

The evaluation of the LS hazard sensitivity map was performed using Receiver Operating Characteristic (ROC) curve analysis.

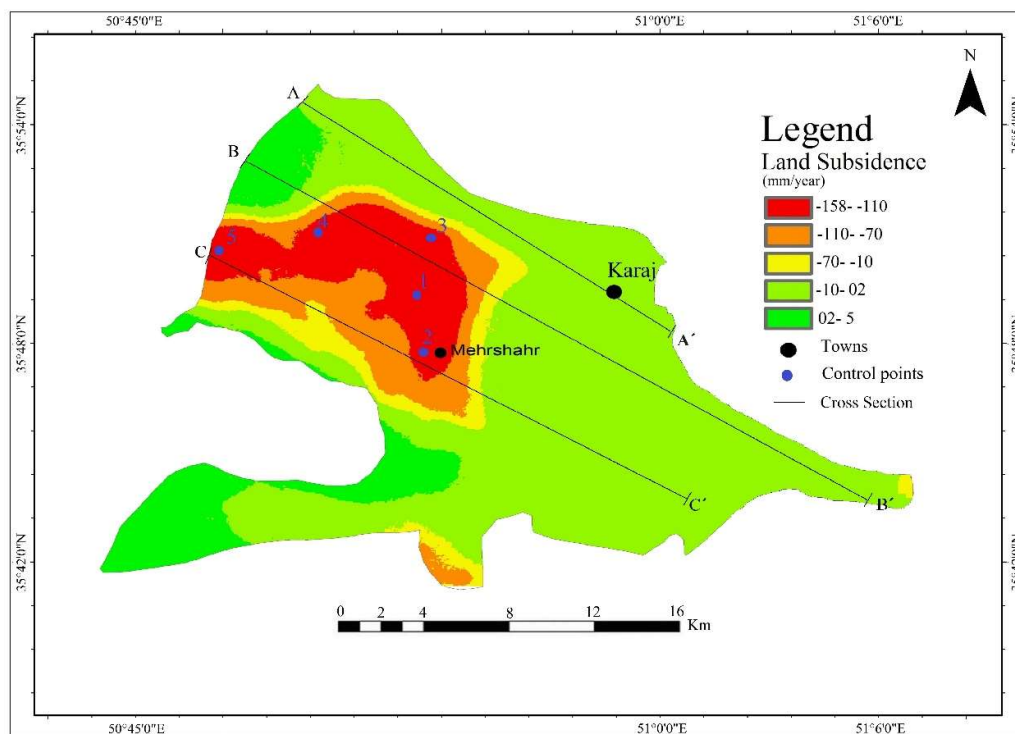


Figure 9. The vertical annual displacement during the years 2014-2023

The analysis of ROC curves is a practical method for evaluating the effectiveness of spatial models. The optimal outcome is a curve that has the highest area under the curve (AUC), which can range from 0.5 to 1.0. An AUC of 0.5 suggests that the model performs no better than chance, while a higher AUC indicates better performance (Fawcett, 2006).

In this research, the vertical displacement map was divided into 30 parts by ArcGIS software to generate the ROC curve. An inventory dataset was produced by extracting the conditions that correspond to zero and larger displacement values. A reference spatial data layer was then created, consisting of two active cells representing pixels with high and lower hazard sensitivity values. The percentages of true positive (TP) and false positive (FP) were computed using SPSS software. The probability image was generated using an LS hazard sensitivity map index that was created through the AHP method. The outcomes of the analysis were stored in a text document, and the ROC curve was generated utilizing dedicated software (Figure 10).

In the ROC curve, the vertical and horizontal axes demonstrate the true and false positive rates, respectively. The true positive rate indicates the proportion of correctly labeled pixels based on the model result, while the false positive rate represents the proportion of incorrectly labeled pixels. The obtained AUC result of 0.773 shows a reasonable level of performance. To validate the accuracy of our method and its percentage, we will examine two similar studies. Jakarta's LS risk was mapped using time-series InSAR on Sentinel-1 data. While all models (AUC > 0.5) offered valuable insights, machine learning models with AdaBoost performing best (AUC: 0.811) were used to analyze the data and create a LS susceptibility map based on ROC curve analysis (Hakim et al., 2020). Mohammady et al. (2019) employed a Random Forest machine learning approach to evaluate the likelihood of LS. The analysis revealed that factors like proximity to faults, elevation, slope variations, land usage patterns, and water table depth significantly influence subsidence. The model's accuracy was evaluated using a receiver operating characteristic curve (ROC), and the resulting area under the curve (AUC) of 0.77 indicated that Random Forest is a suitable method for mapping LS susceptibility in the investigated region.

Discussion

To compare the trends of LS and groundwater level decline in the Karaj plain, five control points were divided into four two-year periods between 2015 and 2023. The locations of the five points are shown in Figure 9. Figures 11 and 12 compare aquifer hydrograph levels to average annual rainfall and LS levels, respectively.

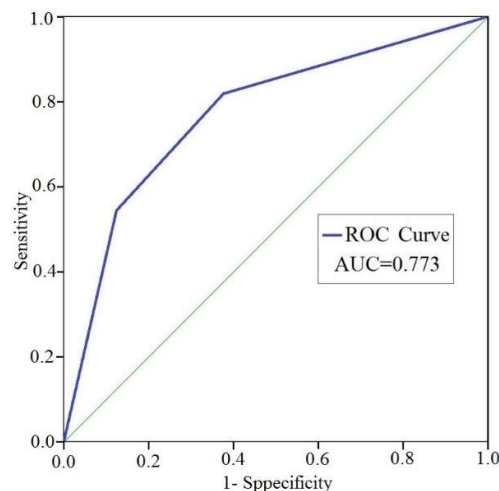


Figure 10. The Roc curve graph for evaluating the performance of the LS hazard sensitivity map

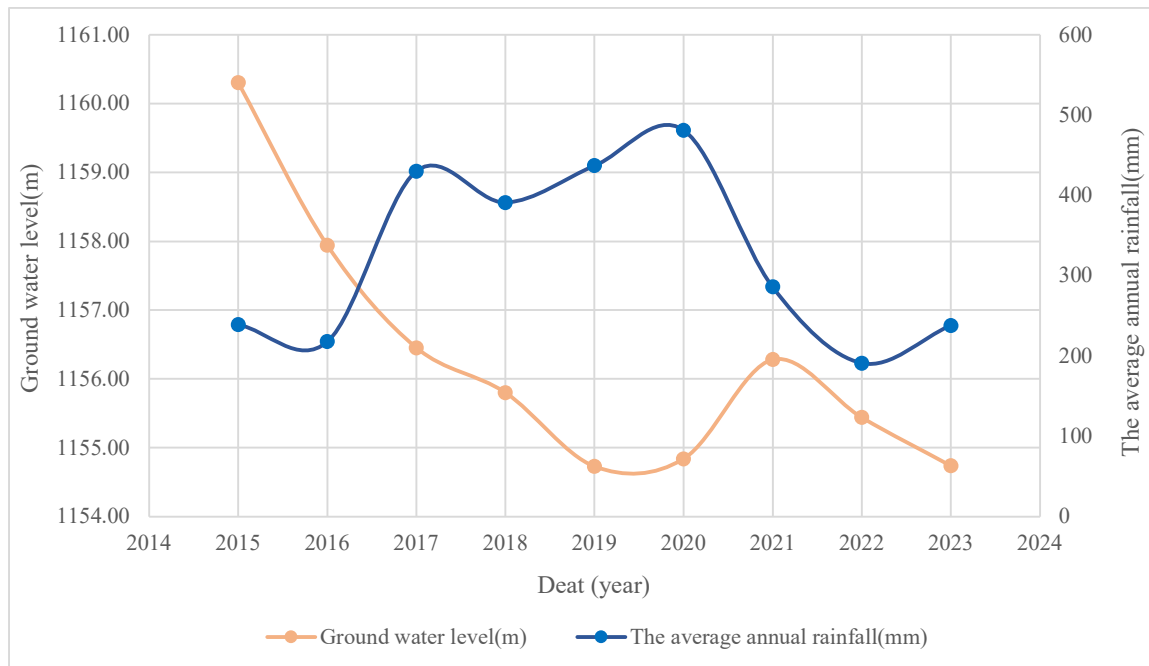


Figure 11. Trends in groundwater level and average annual rainfall (Regional Water Company of Alborz, 2024)

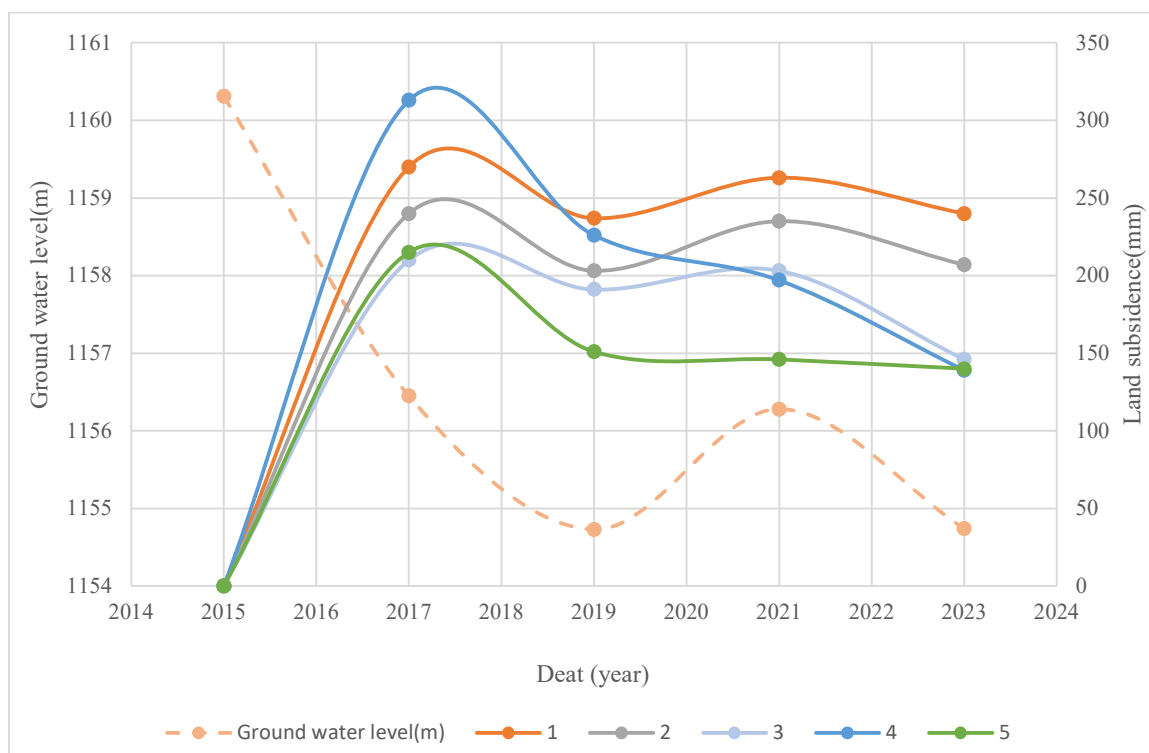


Figure 12. Time series of vertical displacement at control points versus changes in groundwater level

Despite a direct relationship between precipitation rate and groundwater level, changes in groundwater level occur with a lag of several months after an increase or decrease in precipitation rate (Regional Water Company of Alborz, 2024). In general, the rate of LS in the Karaj Plain increases as the water Table. decreases, with a lag of about two years. The highest rate of LS in all five points occurred in 2017, due to a decrease in precipitation in 2015 and

2016 and an increase in groundwater abstraction. The rate of LS in all five points decreased in 2019, due to the increase in precipitation from 2017 to 2019, followed by a decrease in groundwater abstraction and a relative increase in the water Table. However, the highest amount of precipitation in 2020 resulted in an increase in groundwater level in 2021, and this effect is more noticeable in the reduction of subsidence in points 4 and 5. In 2023, the rate of LS shows a slight decrease, likely due to the slight increase in precipitation. Therefore, points 1 and 2 still have a high rate of LS. Control points exhibit a strong positive correlation, ranging from 88% to 99%. Additionally, a significant negative correlation of 66% to 88% is observed between groundwater decline and control points (Table 4). LS in this area exhibits linear behavior and will continue at the same rate until the soil reaches the secondary consolidation stage.

Remote sensing and geographic information systems (GIS) are powerful tools for mapping and assessing natural hazard susceptibility in recent years (e.g. Abedini & Tulabi, 2018; Goorabi, 2020). The hazard sensitivity maps made by these technologies, provide crucial information for comprehending the likelihood of disasters in regions susceptible to LS. This paper focuses on the LS hazard disaster assessment in the Karaj Plain, situated in the central Alborz region of Iran. The study utilizes an integrated approach combining the DInSAR and AHP methods. This research aims to create hazard susceptibility maps by utilizing an integrated approach. These maps will provide valuable information for risk management strategies and assist in the planning and construction of new infrastructure and settlements in regions prone to hazards.

Table 4. Correlation between control points and groundwater drop

Correlation	Ground water level(m)	1	2	3	4	5
Ground water level(m)	1					
1	-0.882	1				
2	-0.863	0.999	1			
3	-0.817	0.977	0.979	1		
4	-0.665	0.879	0.883	0.933	1	
5	-0.775	0.950	0.952	0.951	0.968	1

Conclusion

The objective of this study is to illustrate the application of AHP and DInSAR methods in evaluating areas at risk of LS. No prior efforts have been undertaken to create LS hazard sensitivity maps by integrated AHP methodologies in the studied area. In this research, LS hazard susceptibility maps for the entire study area were created. The AHP-based hazard susceptibility map identified that 33.2% of the Karaj Plain falls within the high-to-very-high risk category for LS. Based on the results of the presented model, distance from fault and permeability have the least impact on LS, while soil texture and groundwater drawdown have the most impact on this parameter. The maximum LS has been observed in the central and northwestern regions of the plain, particularly in layers with thicknesses ranging from 200 to 300 meters that contain significant clay layers. In the west of the study area, there is a likelihood of the existence of a two-layered aquifer. The water level reported by piezometers is significantly lower than the actual water Table. Therefore, piezometers in the central portion of the plain were removed from the first aquifer layer (Recent Sediments), because the first layer is likely a perched aquifer, and the second aquifer layer (unconfined) is likely to play a major role in LS. This factor has negatively impacted the accuracy of the LS Hazard Sensitivity Map and, consequently, its ROC curve.

This study demonstrates that geological factors also significantly influence the rate and pattern of LS observed in the area. While precipitation rate directly influences groundwater level, changes in groundwater level exhibit a time delay of several months following fluctuations in precipitation. The correlation between groundwater depletion and subsidence exhibits a two-year time lag. This suggests that the maximum soil consolidation occurs after a two-year lag in response to groundwater level decrease. The analysis of the control points reveals a strong positive correlation of 88% to 99%. Notably, Points 1 and 2, located in the central portion of the plain, continue to exhibit a high rate of LS.

The accuracy of these maps was assessed using the ROC curve. In light of comparable studies and validation percentages considering various parameters, the validation results with an AUC of 0.773 demonstrated significant effectiveness.

Acknowledgments

We would like to thank the Regional Water Company of Alborz for providing the basic data required for this study.

References

- Abdolali, A., 1991. Resources and water problems of Karaj. Master's thesis, University of Tehran.
- Abdollahi, S., Pourghasemi, H.R., Ghanbarian, G.A., Safaeian, R., 2019. Prioritization of effective factors in the occurrence of Land subsidence susceptibility mapping using an SVM model and different kernel functions: A case study in Kerman province, Iran. *Bulletin of Engineering Geology and the Environment* 77(4): 1791-1807.
- Abedini, M., Tulabi, S., 2018. Assessing LNRF, FR, and AHP models in landslide susceptibility mapping index: a comparative study of Nojian watershed in Lorestan province, Iran. *Environmental Earth Sciences*. <https://doi.org/10.1007/s12665-018-7524-1>.
- Ahmadi, S., Afshar, R.S., Fathollahy, M., Vakili, K.N., 2023. Identification of land subsidence hazard in Asadabad Plain using the PS-InSAR method and its relationship with the geological characteristics. *Natural Hazards*, 1-11. <https://doi.org/10.1007/s11069-023-05963-6>.
- Bagheri-Gavkosh, M., Hosseini, S.M., Ataie-Ashtiani, B., Sohani, Y., Ebrahimian, H., Morovat, F., Ashrafi, S., 2021. Land subsidence: A global challenge. *Science of the Total Environment* 778:146193. <https://doi.org/10.1016/j.scitotenv.2021.146193>.
- C.G.G, Company., 1964-1965. Geophysical Studies of Tehran. Tehran, Iran.
- Chatterjee, R.S., Pranjali, P., Kannaujiya, S., Thapa, S., Bhardwaj, A., Kapoor, U., Dwivedi, S.N., Chandra, R., Srivastava, R.K., Singh, S.K., Kumar, H., Bhattacharjee, R., Singha, S., Kala, S., Kumar, A., 2023. Unravelling the dynamics and causes of land subsidence in the National Capital Territory of Delhi, India, by spaceborne and in situ observations. *Bulletin of Engineering Geology and the Environment*, 82(2): 413-428.
- Chen, H., Hwang, C., Tanaka, Y., Chang, P.Y., 2023. Gravity estimation of groundwater mass balance of sandy aquifers in the LS-hit region of Yunlin County, Taiwan. *Engineering Geology*. DOI: 10.1016/j.enggeo.2023.107021.
- Ciampalini, A., Bardi, F., Bianchini, S., Frodella, W., Del Ventisette, C., Moretti, S., Casagli N., 2014. Analysis of building deformation in landslide area using multisensor PSInSAR™ technique. *Int J Appl Earth Obs Geoinf* 33:166-180.
- Davydzenka, T., Tahmasebi, P., Shokri, N., 2024. Unveiling the global extent of land subsidence: The sinkingcrisis. *Geophysical Research Letters*, 51, e2023GL104497. <https://doi.org/10.1029/2023GL104497>.
- Elmahdy, S.I., Mohamed, M.M., Ali, T.A., Abdalla, J.E. D., Abouleish, M., 2022. Land subsidence and sinkholes susceptibility mapping and analysis using random forest and frequency ratio models in Al Ain, UAE. *Geocarto International*, 37(1): 315-331.
- Faryabi, M., Ghasemi, A., Mohammadi, M., 2023. A fuzzy logic approach for land subsidence susceptibility mapping: The use of hydrogeological data. *Environmental Earth Sciences* 79:1-13.

- Fawcett, T., 2006. An introduction to ROC analysis. *Pattern Recogn. Lett.* 27 (8): 861-874.
- Geological Survey and Mineral Exploration of Iran., 2020. A study on the risks of land subsidence in Tehran province (Karaj plain). Tehran, Iran: Geological Survey of Iran. [Report in the third volume of geological water report].
- Ghabadi, M.H., 2013. Groundwater. Hamedan: University of Bu Ali Sina. 320 pp.(in Persian).
- Goorabi, A., 2020. Detection of landslide induced by large earthquake using InSAR coherence techniques – Northwest Zagros Iran. *Egypt J Remote Sens Space Sci* 23:195-205.
- Hakim, W.L., Achma, A.R., Lee, C.W., 2020. Land subsidence susceptibility mapping in Jakarta using functional and meta-ensemble machine learning algorithm based on time-series InSAR data. *Remote Sensing*, 12(21): 1–26.
- Hoffmann, J., Zebker, H.A Galloway, D.L., Amelung, F., 2001. Seasonal subsidence and rebound in Las Vegas Valley, Nevada, observed by synthetic aperture radar interferometry. *Water Resour Res* 37:1551-1566.
- Hussain, M.A., Chen, Z., Khan, J., 2024. Monitoring land subsidence in the Peshawar District, Pakistan, with a multi-track PS-InSAR technique. *Environmental Science and Pollution Research*, 1-14. <https://doi.org/10.1007/s11356-024-31995-x>.
- Ilija, I., Loupasakis, C., Tsangaratos, P., 2018. Land subsidence phenomena investigated by spatiotemporal analysis of groundwater resources, remote sensing techniques, and random forest method: The case of Western Thessaly, Greece. *Environmental Monitoring and Assessment*, 190(11): 623. <https://doi.org/10.1007/s10661-018-6992-9>.
- Jahangir, M.H., Khosravi, Z., Sarrafha, H., 2020. Modeling of land subsidence due to groundwater overexploitation using elastoplastic Mohr-Coulomb model in Arak plain, Iran. *Geopersia*, 11(1): 131-151.
- Khezri, M., Heidarzadeh, Gh., Shahidi, A., Oroujnia, P., Vakil Baghmishch, F., Ghaemi, J., Haddadan, M., 2023. Geologic map of the Alborz Quadrangle, County Karaj, Geological Map of Iran Sheet Number- 6161 I SE, scale I: 25,000.
- Li, X., Li, Y., 2023. Study on land subsidence characteristics and deformation evolution mechanism in Caofeidian New Area, Bohai Bay. *Bulletin of Engineering Geology and the Environment*, 82(2): 96-107.
- Li, Y., Gong, H., Zhu, L., Li, X., 2017. Measuring spatiotemporal features of LS, groundwater drawdown, and compressible layer thickness in Beijing Plain. *China Water* 9: 64.
- Mahmoudpour, M., Khamsehchiyan, M., Nikudel, M.R., Ghassemi, M.R., 2016. Numerical simulation and prediction of regional land subsidence caused by groundwater exploitation in the southwest plain of Tehran, Iran. *Eng Geol* 201:6–28.
- Mehrnoor, S.M., Rabati, M., Kheirvakh Zare Kash, M., Farsad, F., Bikpour, S., 2023. Zoning of land subsidence hazard in Hesarak Plain based on an integrated multi-criteria decision-making approach: WOI-BWM. *Journal of Geography and Environmental Hazards*, 11(2): 27-148.
- Mohammady, M., Pourghasemi, H.R., Amiri M., 2019. Land subsidence susceptibility assessment using random forest machine learning algorithm. *Environmental Earth Sciences*, 78 (16): 503. <https://doi.org/10.1007/s12665-019-8518-3>.
- Motagh, M., Walter, R.T., Sharifi, M.A., Fielding, E., Schenk, A., Anderssohn, J., Zschau, J., 2008. LS in Iran caused by widespread water reservoir over exploitation. *Geophysical Research Letters* 35: 403-412.
- Ozdemir, A., 2016a. Investigation of sinkholes spatial distribution using the weights of evidence method and GIS in the vicinity of Karapinar (Konya, Turkey). *Geomorphology*, 245: 40-50.
- Ozdemir, A., 2016b. Sinkhole susceptibility mapping using logistic regression in Karapinar (Konya, Turkey). *Bulletin of Engineering Geology and the Environment* 75:681-707.
- Pepe, A., Calò, F., 2017. A review of interferometric synthetic aperture RADAR (InSAR) multi-track approaches for the retrieval of Earth's surface displacements. *Applied Sciences* 7: 1264. <https://doi.org/10.3390/app7121264>.
- Rahmani, P., Gholami, H., Golzari, S., 2024. An interpretable deep learning model to map land subsidence hazard. *Environmental Science and Pollution Research*, 1-14. <https://doi.org/10.1007/s11356-024-32280-7>.
- Ranjbar Barough, Z., Fathollahzadeh, M., 2023. Investigating land subsidence using time series of radar images and its relationship with groundwater level changes (Case study: Karaj metropolis).

- Quantitative Geomorphology Research, 10(4): 138-155.
- Regional Water Company of Alborz., 2019. Statistics and basic information on water resources (Implementation of an Integrated Management System). Retrieved from <https://www.abfa-alborz.ir/> (in Persian).
- Regional Water Company of Alborz., 2022. Statistics and basic information on water resources. Retrieved from <https://www.albrw.ir/> (in Persian).
- Regional Water Company of Alborz., 2024. Rainfall statistics based on stations...<https://www.albrw.ir> (in Persian).
- Rezaeia, M., Noorib, Z.Y., Barmakib, M. D., 2020. Land subsidence susceptibility mapping using Analytical Hierarchy Process (AHP) and Certain Factor (CF) models at Neyshabur plain, Iran. *GEOCARTO INTERNATIONAL*, 29(5): 643-656.
- Rieben H., 1955. The Geology of the Tehran Plain. *American Journal of Science* 253:617-639. <https://doi.org/10.2475/ajs.253.11.617>.
- Riseh, Y.A., Rajabi, A.M., Edalat, A., 2023. Modeling of land subsidence induced by groundwater withdrawal using Artificial Neural Network (A case study in central Iran). *Geopersia*, 13(1), 67-81. <https://doi.org/10.22059/GEOPE.2022.350610.648687>.
- Saaty, T. L., 1980a. The analytic hierarchy process: planning. *Priority Setting. Resource Allocation*, MacGraw-Hill, New York International Book Company.
- Saaty, T. L., 1977. A scaling method for priorities in hierarchical structures. *Journal of Mathematical Psychology* 15: 234-281.
- Saaty, T. L., 1980b. The analytical hierarchy process, planning, priority. In *Priority Setting. Resource Allocation*, MacGraw-Hill, New York International Book Company.
- Safari, H., Jafari, F., Tawakli Sabor, S.M., 2016. Land subsidence monitoring and its relationship with groundwater withdrawal: A case study: Karaj- Shahriar. *Journal of Quantitative Geomorphology Research*, 5(2): 82-93.
- Salehi Moteahd, F., Hafezi Moghaddas, N., Lashkaripour, G.R., Dehghani, M., 2019. Geological parameters affected LS in Mashhad plain, north-east of Iran. *Environmental Earth Sciences* 78: 405. <https://doi.org/10.1007/s12665-019-8413-y>.
- Shahoriar Sarker, M.d., Maksud Kamal, A. S. M., Zillur Rahman, M.d., Faruki Fahim, A.K., 2024. Land subsidence monitoring using InSAR technique in the southwestern region of Bangladesh, *Geomatics, Natural Hazards and Risk*, 15:1, 2333795. <https://doi.org/10.1080/19475705.2024.2333795>.
- Shastri, A., Sreejith, K.M., Rose, M.S., Agrawal, R., Sunil, P.S., Sunda, S., Chaudhary, B.S., 2023. Two decades of land subsidence in Kolkata, India revealed by InSAR and GPS measurements: implications for groundwater management and seismic hazard assessment. *Natural Hazards*, 118(3): 2593-2607.
- Smith, R.G., Majumdar, S., 2020. Groundwater storage loss associated with land subsidence in western United States mapped using machine learning. *Water Resources Research*, 56(7), e2019WR026621. <https://doi.org/10.1029/2019WR026621>.
- The Statistical Center of Iran., 2021. Population and Housing Census. Tehran: The Statistical Center of Iran (in Persian).
- Ty, T.V., Minh, H. V. T., Avtar, R., Kumar, P., Hiep, H.V., Kurasaki, M., 2021. Spatiotemporal variations in groundwater levels and the impact on land subsidence in Can Tho, Vietnam. *Groundwater for Sustainable Development*. <https://doi.org/10.1016/j.gsd.2021.100680>.
- USGS., 2023. Land subsidence. Retrieved September 6, 2023, from <https://www.usgs.gov/special-topics/water-science-school/science/land-subsidence>.
- Wang, YQ., Wang, ZF., Cheng, WC., 2019. A review on LS caused by groundwater withdrawal in Xi'an, China. *Bulletin of Engineering Geology and the Environment* 78:2851-2863.
- Zhang, L., Arabameri, A., Santosh, M., Pal, SC., 2023. Land subsidence susceptibility mapping: Comparative assessment of the efficacy of five models. *Environmental Science and Pollution Research*, 30(77), 77830-77849. doi.org/10.1007/s11356-023-27799-0.
- Zhao, R., Arabameri, A., Santosh, M., 2024. Land subsidence susceptibility mapping: a new approach to improve decision stump classification (DSC) performance and combine it with four machine learning algorithms. *Environmental Science and Pollution Research*, 1-14. <https://doi.org/10.1007/s11356-024-32075-w>.
- Zheng, M., Guo, Q., Zhao, R., Wang, L., Han, Y., 2023. Surface subsidence disasters over Xuzhou city,

- China 2014–2018 revealed by InSAR and Peck model. *Environmental Earth Sciences* 82: 264.
- Zhou, C., Lan, H., Gong, H., Zhang, Y., Warner, T.A., Clague, J.J., Wu, Y., 2020. Reduced rate of LS since 2016 in Beijing, China: evidence from Tomo-PSInSAR using RadarSAT-2 and Sentinel-1 datasets. *International Journal of Remote Sensing* 41:1259-1285.
- Zuccarini, A., Giacomelli, S., Severi, P., Berti, M., 2023. Long-term spatiotemporal evolution of land subsidence in the urban area of Bologna, Italy. *Bulletin of Engineering Geology and the Environment*, 83 (1): 35. <https://doi.org/10.1007/s10064-023-03517-5>.



This article is an open-access article distributed under the terms and conditions of the Creative Commons Attribution (CC-BY) license.